Journal of Hydraulic Research Vol. 44, No. 3 (2006), pp. 402–411

A third-order explicit central scheme for open channel flow simulations

Un modèle explicite central du troisième ordre pour des simulations d'écoulement en canal a surface libre

M. VENUTELLI, *Department of Civil Engineering, University of Pisa, Pisa, Italy*

ABSTRACT
A third-order explicit time-stepping model for the simulations in open channels flow is presented. The time discretization of one-dimensional Saint-Venant's basic equations is obtained by Taylor series expansion, formulated in multi-stage approach, whereas the spatial discretization is obtained by finite difference central scheme. First- and second-order models have been obtained by using piecewise constant and piecewise linear MUSCL (monotone upwind scheme for conservation laws) approximations. Afterwards, the third-order model proposed is obtained by a piecewise quadratic polynomial approximation. Using Fourier's linear analysis, the stability and the accuracy of the scheme are investigated. The numerical results, for predicting dam-break in a horizontal and frictionless channel and for the representation of the hydraulic jump in prismatic and non-prismatic channels, with non-uniform bottom slope, are evaluated, and compared with the corresponding analytical and measured solutions.

RÉSUMÉ
On a présenté un modèle explicite du troisième ordre en temps fractionné pour des simulations de flux dans des canaux ouverts. Dans ce modèle, les équations de base forment un système de Saint-Venant unidimensionnel et sont d'abord discrétisées par rapport au temps, avec un développement en série de Taylor formulé en plusieurs phases. Les équations ainsi obtenues sont alors discrétisées dans l'espace à l'aide de réseaux centraux aux différences finies. En utilisant des polynômes constants et linéaires MUSCL (schéma amont monotone pour les lois de conservation) on à obtenu respectivement un modèle du premier et du deuxième ordre. Ensuite, en utilisant des polynômes quadratiques on à trouvé le modèle du troisième ordre proposé. Avec l'analyse linéaire de Fourier, sont recherché la stabilité et la précision du schema. Les résultats numériques, pour des simulations de rupture de barrage dans des canaux horizontaux et sans frottement et, pour la représentation du ressaut hydraulique, dans des canaux prismatiques et non prismatiques avec une pente variable du fond, est en accord avec les solutions analytiques correspondantes.

Keywords: Saint-Venant equations, Taylor expansion, central difference schemes, stability, shock phenomena.

1 Introduction

In many cases concerning hydraulic and environmental engineering, a correct representation of the water depth and velocity, consequent to rapidly varied flows, resulting from a dam-break or a hydraulic jump, is necessary. The mathematical description of these phenomena, in the hypothesis of hydrostatic pressure distribution and small bottom slope, is the set of non-homogeneous Saint-Venant equations. These equations, which are hyperbolic and non-linear, except in simplified cases, can only be solved numerically.

The numerical schemes used, the so-called shock-capturing schemes, should be able to simulate the rapid variations of the hydraulic characteristics accurately, without introducing any spurious oscillations. A large class of these schemes have been obtained by using Godunov's method in "upwind" approach (Hirsch, 1995). Several formulations, using Riemann solvers, have been presented. First-order explicit model, obtained by using Roe's numerical flux and second-order extension, obtained by using Lax-Wendroff numerical flux are proposed by Jha *et al.* (1995), while Delis *et al.* (2000a) present and compare four approximate Riemann solvers. According to the total variation diminishing (TVD) introduced by Harten (1983), a variety of high-resolution explicit and implicit schemes are presented by Delis and Skeels (1998), Delis *et al.* (2000b), and Tseng *et al.* (2001). A second-order scheme, using a Godunov-type finite volume method is presented by Sanders (2001). Unlike upwind schemes, which compute the reconstructed values at the mid-cells, the Godunov-type central schemes compute the staggered cell averages at the interfacing breakpoints. Therefore, the central schemes present the advantage of simplicity, since no Riemann solvers are involved in their construction. The forerunner central scheme is the first-order Lax–Friedrichs scheme (Lax, 1954; Friedrichs, 1954). Its second-order staggered extension was

Revision received July 19, 2005/Open for discussion until May 31, 2007.

proposed by Nessyahu and Tadmor (1990). For the solution of the homogeneous convection and of the convection–diffusion equations, second-order new schemes have recently been introduced by Kurganov and Tadmor (2000).

In this paper, a third-order central scheme in explicit time-stepping formulation is proposed for the solution of the non-homogeneous system of Saint-Venant equations. The discretization in time, with Taylor expansions, is based on fractional step, while the spatial approximation is obtained by using a piecewise quadratic polynomial. The results of shocks simulations are presented in open-channel flows as a consequence of the dam-break and of the hydraulic jump phenomena. The same tests are carried out even by first- and second-order models, which have been obtained by using piecewise-constant and piecewise-linear MUSCL (Monotone Upwind Scheme for Conservation Laws) approximations, respectively. The paper is organized as it follows: the Saint-Venant governing equations of the unsteady flow in open-channel are reported in the Section 2, the numerical formulation and the stability analysis of the model are presented in the Section 3, the numerical applications are described in the Section 4 and the conclusions of the work are reported in the Section 5.

2 Governing equations

The one-dimensional unsteady flow in open-channel is governed by a system of Saint-Venant equations (Cunge *et al.*, 1980)

$$\frac{\partial u}{\partial t} + \frac{\partial f(u)}{\partial x} = z(u) \tag{1}$$

where,

$$u = \begin{pmatrix} A \\ Q \end{pmatrix}, \quad f = \begin{pmatrix} Q \\ \frac{Q^2}{A} + gI_1 \end{pmatrix},$$

$$z = \begin{pmatrix} 0 \\ gI_2 + gA(S_0 - S_f) \end{pmatrix},$$

with $A = A(x, t)$ the wetted cross-sectional area, $Q = Q(x, t)$ is the discharge, g is the gravitational acceleration, x is the spatial coordinate, assumed positive along the flow direction, and t is the time. The term I_1 represents the hydrostatic pressure force, while I_2 represents the pressure forces due to the longitudinal width variations, expressed as

$$I_1 = \int_0^{h(x,t)} (h - \eta)\sigma(x, \eta)\, \mathrm{d}\eta,$$

$$I_2 = \int_0^{h(x,t)} (h - \eta)\frac{\partial \sigma(x, \eta)}{\partial x}\, \mathrm{d}\eta$$

where, h is the water depth, η is the depth integration variable along the vertical axis, σ is the width of the cross-section such that $\sigma(x, h) = b(x) =$ free surface width. In case of non-prismatic rectangular channel, one obtains

$$I_1 = \frac{A^2}{2b}, \quad I_2 = \frac{A^2}{2b^2}\frac{\mathrm{d}b}{\mathrm{d}x}$$

In the end, S_0 is the bed slope, and S_f is the friction slope in the vector z of source terms. According to Manning's formula for the evaluation of S_f, we have $S_\mathrm{f} = n_m^2 Q|Q|/(A^2 R^{4/3})$ in which $n_m(\mathrm{m}^{-1/3}\mathrm{s})$ is the roughness coefficient and $R = A/P$ hydraulic radius with $P =$ wetted perimeter.

The system (1) must be completed with the initial and appropriate boundary conditions. Taken, for the dependent variables A and Q, the spatial domain $\Omega \equiv (0, L)$ in general one obtains

$$A(x, 0) = A_0(x), \quad Q(x, 0) = Q_0(x),$$

$$\begin{cases} Q(0, t) = Q^*(t), \\ A(L, t) = A^*(t) \end{cases}$$

where $Q^*(t)$ and $A^*(t)$ must be known functions.

3 Numerical model

3.1 Time integration

For time integration of system (1), from $t^n = n\Delta t$ to $t^{n+1} = t^n + \Delta t$, according to Taylor series expansion, it results

$$u^{n+1} = u^n + \Delta t\left(\frac{\partial u}{\partial t}\right)^n + \frac{1}{2}(\Delta t)^2\left(\frac{\partial^2 u}{\partial t^2}\right)^n + \frac{1}{6}(\Delta t)^3\left(\frac{\partial^3 u}{\partial t^3}\right) + \cdots = \exp\left(\Delta t\frac{\partial}{\partial t}\right)u^n \tag{2}$$

from which one observes that the evolution operator $E(\Delta t) : u(t^n) \to u(t^{n+1})$ is given by the exponential function $\exp(s)$, where $s = \Delta t(\partial/\partial t)$. It is therefore apparent that general, explicit and implicit schemes of various order of accuracy can be devised in the form of Padé approximations to the exponential function (Butcher, 1987; Donea *et al.*, 2000).

In order to implement the expansion (2) in this work, in third-order explicit approximation, involving only first time derivatives, it is convenient to express the Eq. (2) in factorized form

$$u^{n+1} = \left(1 + s\left(1 + \frac{1}{2}s\left(1 + \frac{1}{3}s\right)\right)\right)u^n$$

from which a three stages scheme is obtained

$$u^{n+1/3} = u^n + \frac{1}{3}\Delta t\left(\frac{\partial u}{\partial t}\right)^n \tag{3}$$

$$u^{n+1/2} = u^n + \frac{1}{2}\Delta t\left(\frac{\partial u}{\partial t}\right)^{n+1/3} \tag{4}$$

$$u^{n+1} = u^n + \Delta t\left(\frac{\partial u}{\partial t}\right)^{n+1/2} \tag{5}$$

3.2 Spatial integration

3.2.1 Central schemes

One considers the system (1) in homogeneous form

$$\frac{\partial u}{\partial t} + \frac{\partial f(u)}{\partial x} = 0 \tag{6}$$

By applying Eq. (3), which represents the first stage of the time stepping algorithm, and with the integration on spatial domain

$\Omega_x := [x-\Delta x/2, x+\Delta x/2]$, with Δx space interval, one obtains

$$\bar{u}(x, t^{n+1/3}) = \bar{u}(x, t^n) - \frac{1}{3}\lambda\left[f\left(u\left(x+\frac{\Delta x}{2}, t^n\right)\right) - f\left(u\left(x-\frac{\Delta x}{2}, t^n\right)\right)\right] \quad (7)$$

where

$$\bar{u}(x,t) = \frac{1}{\Delta x}\int_{x-\Delta x/2}^{x+\Delta x/2} u(x,t)\,\mathrm{d}x$$

indicates the sliding average of $u(\cdot, t)$, and $\lambda = \Delta t/\Delta x$. Therefore one constructs a piecewise approximation $w(\cdot, t^n)$ of $u(\cdot, t^n)$ at the discrete time level $t^n = n\Delta t$

$$u(x, t^n) \cong w(x, t^n) = \sum_j p_j(x) 1_{I_j} \quad (8)$$

where $p_j(x)$ are algebraic polynomials supported at the discrete cells $I_j := [x_{j-1/2}, x_{j+1/2}]$ centred around the mid-points $x_j = j \cdot \Delta x$, and 1_{I_j} is a function which equals one inside I_j and zero outside I_j. The time evolution of the piecewise approximation $w(x, t^n)$, on the basis of the Eq. (7), becomes

$$\bar{w}(x, t^{n+1/3}) = \bar{w}(x, t^n) - \frac{1}{3}\lambda\left[f\left(w\left(x+\frac{\Delta x}{2}, t^n\right)\right) - f\left(w\left(x-\frac{\Delta x}{2}, t^n\right)\right)\right] \quad (9)$$

Equation (9) is then applied to the discrete grid points. Here, we distinguish between two main methods, corresponding to the upwind and central schemes, respectively, according to the way sampling Eq. (9) (Liu and Tadmor, 1998). Upwind schemes were based on sampling Eq. (9) at the mid-cells $x = x_j$. This scheme use non-staggered grid-cells $[x_{j-1/2}, x_{j+1/2}]$ and they depend upon the solution of exact or approximate Riemann problem solvers at the grid-cell interfaces, for the calculation of the numerical fluxes. In contrast, central schemes are based on sampling Eq. (9) at the interfacing breakpoints $x = x_{j+1/2}$. In this case, the space integration is carried out on staggered grid-cells $[x_j, x_{j+1}]$, and one obtains

$$\bar{w}^{n+1/3}_{j+1/2} = \bar{w}^n_{j+1/2} - \frac{1}{3}\lambda[f(w(x_{j+1}, t)) - f(w(x_j, t))] \quad (10)$$

in which the staggered averages $\bar{w}^n_{j+1/2}$ are given by

$$\bar{w}^n_{j+1/2} = \frac{1}{\Delta x}\left[\int_{x_j}^{x_{j+1/2}} p_j(x)\,\mathrm{d}x + \int_{x_{j+1/2}}^{x_{j+1}} p_{j+1}(x)\,\mathrm{d}x\right] \quad (11)$$

Different schemes can be obtained by changing the polynomial representation $p_j(x)$ the variables within each grid-cell. By using, within the cell $[x_{j-1/2}, x_{j+1/2}]$ piecewise-constant approximation $p_j(x) = \bar{w}^n_j$, and piecewise-linear MUSCL approximation $p_j(x) = \bar{w}^n_j + w'_j(x - x_j)/\Delta x$, where w'_j indicates the discrete first-derivative (van Leer, 1979), a first- and second-order schemes are obtained, respectively. In the end, by using quadratic polynomial, a third-order scheme, which will be treated afterwards, is obtained.

3.2.2 Third-order central scheme

For the realization of the third-order central scheme, the quadratic polynomial $p_j(x)$ proposed by Liu and Tadmor (1998) is used

$$p_j(x) = (1 - \vartheta_j)\bar{w}^n_j + \vartheta_j q_j(x) \quad (12)$$

where $\vartheta_j\,(0 < \vartheta_j < 1)$ is a non-linear limiter, $\bar{w}^n_j$ the cell averages, and $q_j(x)$ the quadratic polynomial

$$q_j(x) = a_j + b_j\left(\frac{x - x_j}{\Delta x}\right) + c_j\left(\frac{x - x_j}{\Delta x}\right)^2$$

Assuming that $q_j(x)$ interpolates $\bar{w}^n_j$ and, in addition, interpolates two neighbouring cell averages $\bar{w}^n_{j\pm1}$, one obtains

$$q_j(x) = \left(\bar{w}^n_j - \frac{1}{24}\Delta_+\Delta_-\bar{w}^n_j\right) + \Delta_0\bar{w}^n_j\left(\frac{x - x_j}{\Delta x}\right) + \frac{1}{2}\Delta_+\Delta_-\bar{w}^n_j\left(\frac{x - x_j}{\Delta x}\right)^2$$

where,

$$\Delta_\pm w(x) = \pm(w(x \pm \Delta x) - w(x))$$

and

$$\Delta_0 = \frac{1}{2}(\Delta_+ + \Delta_-)$$

Finally, in Eq. (12), the limiter ϑ_j, which is used in order to prevent the oscillation, is given by the formula (Liu and Osher, 1996; Liu and Tadmor, 1998)

$$\vartheta^n_j := \begin{cases} \min\left\{\dfrac{M_{j+1/2} - \bar{w}^n_j}{M_j - \bar{w}^n_j}, \dfrac{m_{j-1/2} - \bar{w}^n_j}{m_j - \bar{w}^n_j}, 1\right\}, \\ \qquad \text{if } \bar{w}^n_{j-1} < \bar{w}^n_j < \bar{w}^n_{j+1} \\ \min\left\{\dfrac{M_{j-1/2} - \bar{w}^n_j}{M_j - \bar{w}^n_j}, \dfrac{m_{j+1/2} - \bar{w}^n_j}{m_j - \bar{w}^n_j}, 1\right\}, \\ \qquad \text{if } \bar{w}^n_{j-1} > \bar{w}^n_j > \bar{w}^n_{j+1} \\ 1 \quad \text{otherwise} \qquad \left(\text{if } \Delta_+\bar{w}^n_j \cdot \Delta_-\bar{w}^n_j < 0\right) \end{cases} \quad (13)$$

where the cell quantities M and m, it results

$$M^n_j = \max\left\{q^n_j(x_{j+1/2}), q^n_j(x_{j-1/2})\right\}$$
$$M^n_j = \min\left\{q^n_j(x_{j+1/2}), q^n_j(x_{j-1/2})\right\}$$

and

$$M^n_{j+1/2} = \max\left\{\frac{1}{2}\left(\bar{w}^n_j + \bar{w}^n_{j\pm1}\right), q^n_{j\pm1}(x_{j\pm1/2})\right\}$$
$$M^n_{j+1/2} = \min\left\{\frac{1}{2}\left(\bar{w}^n_j + \bar{w}^n_{j\pm1}\right), q^n_{j\pm1}(x_{j\pm1/2})\right\}$$

In the end, the piecewise-quadratic polynomial (12) consists of quadratic pieces of the form

$$p_j(x) = w_j^n + w'_j\left(\frac{x-x_j}{\Delta x}\right) + \frac{1}{2}w''_j\left(\frac{x-x_j}{\Delta x}\right)^2 \tag{14}$$

where the pointvalues w_j^n, and the discrete first w'_j and second w''_j pointvalues derivatives, are given by

$$w_j := \bar{w}_j^n - \frac{1}{24}w''_j \tag{15}$$

$$w'_j := \vartheta_j \Delta_0 \bar{w}_j^n \tag{16}$$

$$w''_j := \vartheta_j \Delta_+ \Delta_- \bar{w}_j^n \tag{17}$$

With $p_j(x)$ specified in the Eqs (14)–(17), by applying Eq. (11), one evaluates the staggered averages of third-order

$$\bar{w}_{j+1/2}^n = \frac{1}{2}(\bar{w}_j + \bar{w}_{j+1}) + \frac{1}{8}(w'_j - w'_{j+1})$$

therefore the Eq. (10), it becomes

$$\begin{aligned}\bar{w}_{j+1/2}^{n+1/3} &= \frac{1}{2}(\bar{w}_j + \bar{w}_{j+1}) + \frac{1}{8}(w'_j - w'_{j+1}) \\ &\quad - \frac{1}{3}\lambda\big[f\big(w_{j+1}^n\big) - f\big(w_j^n\big)\big]\end{aligned} \tag{18}$$

In order to transform the staggered Eq. (18) into a non-staggered, as a first step, we reconstruct a piecewise-quadratic interpolant through the calculated staggered cell-averages at time $t^{n+1/3}$

$$\begin{aligned}\bar{w}_{j\pm1/2}^{n+1/3} &= \bar{w}_{j\pm1/2}^{n+1/3} + (w')_{j\pm1/2}^{n+1/3}\left(\frac{x-x_{j\pm1/2}}{\Delta x}\right) \\ &\quad + \frac{1}{2}(w'')_{j\pm1/2}^{n+1/3}\left(\frac{x-x_{j\pm1/2}}{\Delta x}\right)^2\end{aligned}$$

as, a second step, the cell averages $\bar{w}_j^{n+1/3}$ are obtained by averaging this interpolant, in the following non-staggered equations

$$\begin{aligned}\bar{w}_j^{n+1/3} &= \frac{1}{\Delta x}\left[\int_{x_{j-1/2}}^{x_j} w_{j-1/2}^{n+1/3}\,\mathrm{d}x + \int_{x_j}^{x_{j+1/2}} w_{j+1/2}^{n+1/3}\,\mathrm{d}x\right] \\ &= \frac{1}{4}\big(w_{j-1}^n + 2w_j^n + w_{j+1}^n\big) - \frac{1}{16}(w'_{j+1} - w'_{j-1}) \\ &\quad - \frac{\lambda}{6}[f\big(w_{j+1}^n\big) - f\big(w_{j-1}^n\big)] \\ &\quad + \frac{1}{8}\big((w')_{j-1/2}^{n+1/3} - (w')_{j+1/2}^{n+1/3}\big)\end{aligned} \tag{19}$$

in which the staggered derivatives are given by

$$(w')_{j+1/2}^{n+1/3} = \vartheta_{j+1/2}\frac{1}{2}\big(\bar{w}_{j+3/2}^{n+1/3} - \bar{w}_{j-1/2}^{n+1/3}\big)$$

$$(w')_{j-1/2}^{n+1/3} = \vartheta_{j-1/2}\frac{1}{2}\big(\bar{w}_{j+1/2}^{n+1/3} - \bar{w}_{j-3/2}^{n+1/3}\big)$$

and are evaluated at time level $t^{n+1/3}$ by using Eq. (18). The space discretization is completed by considering Saint-Venant system equations (1) in non-homogeneous form. The source term $z(u)$ is approximated by Simpson's quadrature rule, which is sufficient for retaining third-order accuracy. The Eq. (19) becomes

$$\begin{aligned}\bar{w}_j^{n+1/3} &= \frac{1}{4}\big(w_{j-1}^n + 2w_j^n + w_{j+1}^n\big) - \frac{1}{16}(w'_{j+1} - w'_{j-1}) \\ &\quad - \frac{\lambda}{6}\big[\big(w_{j+1}^n\big) - f\big(w_{j-1}^n\big)\big] \\ &\quad + \frac{1}{8}\big((w')_{j-1/2}^{n+1/3} - (w')_{j+1/2}^{n+1/3}\big) \\ &\quad - \frac{\Delta t}{18}\big(z\big(w_{j-1}^n\big) + 4z\big(w_j^n\big) + z\big(w_{j+1}^n\big)\big)\end{aligned} \tag{20}$$

Equation (20) represents the first stage of the third-order model. Following the same way for the other two stages one obatins, respectively,

$$\begin{aligned}\bar{w}_j^{n+1/2} &= \frac{1}{4}\big(w_{j-1}^n + 2w_j^n + w_{j+1}^n\big) - \frac{1}{16}(w'_{j+1} - w'_{j-1}) \\ &\quad - \frac{\lambda}{4}\big[f\big(w_{j+1}^{n+1/3}\big) - f\big(w_{j-1}^{n+1/3}\big)\big] \\ &\quad + \frac{1}{8}\big((w')_{j-1/2}^{n+1/2} - (w')_{j+1/2}^{n+1/2}\big) - \frac{\Delta t}{12}\big(z\big(w_{j-1}^{n+1/3}\big) \\ &\quad + 4z\big(w_j^{n+1/3}\big) + z\big(w_{i+1}^{n+1/3}\big)\big)\end{aligned} \tag{21}$$

$$\begin{aligned}\bar{w}_j^{n+1} &= \frac{1}{4}\big(w_{j-1}^n + 2w_j^n + w_{j+1}^n\big) - \frac{1}{16}(w'_{j+1} - w'_{j-1}) \\ &\quad - \frac{\lambda}{2}\big[f\big(w_{j+1}^{n+1/2}\big) - f\big(w_{j-1}^{n+1/2}\big)\big] \\ &\quad + \frac{1}{8}\big((w')_{j-1/2}^{n+1} - (w')_{j+1/2}^{n+1}\big) \\ &\quad - \frac{\Delta t}{6}\big(z\big(w_{j-1}^{n+1/2}\big) + 4z\big(w_j^{n+1/2}\big) + z\big(w_{j+1}^{n+1/2}\big)\big)\end{aligned} \tag{22}$$

3.3 Stability analysis

The stability and the accuracy of the third-order three stages scheme, represented by the Eqs (20)–(22), are investigated with the linear Fourier analysis. The one-dimensional linearized Saint-Venant equations (1), are given by

$$\frac{\partial u}{\partial t} + J\frac{\partial u}{\partial x} = Ku \tag{23}$$

where,

$$J = \begin{bmatrix} 0 & 1 \\ c^2 - U^2 & 2U \end{bmatrix}, \quad K = \begin{bmatrix} 0 & 0 \\ g\left(\frac{I_2}{A} + S_0\right) & -r \end{bmatrix}$$

in which $U = Q/A$ is the mean velocity, $c = (gA/b)^{1/2}$ is the celerity, and $r = gS_\mathrm{f}/U$ is the dimensional friction parameter. Assuming a harmonic wave of the form $u = u_0\exp[\mathrm{i}(mx - \beta t)]$, where u_0 is a constant i, is the imaginary unit, m is the dimensional wavenumber, and β is the temporal frequency, after standard procedure (Wesseling, 2001), supposed $I_2 = 0$, from system (23), one obtains

$$\beta_{1,2} = -\mathrm{i}\frac{s}{2} \pm \sqrt{c^2m^2 - \frac{r^2}{4}} + m \cdot u \tag{24}$$

for progressive and retrogressive waves, respectively. From Eq. (24), the analytical amplification factor $g_{a_{1,2}}$ and the analytical phase angle $\phi_{a_{1,2}}$ may be obtained.

For the numerical model, taken the limiter ϑ_j, defined by Eq. (13), equal to 1, after some manipulations, the numerical amplification factors for the two flood waves, result

$$g_{n_{1,2}} = \alpha + \lambda_{1,2}\left(\alpha + \frac{\lambda_{1,2}}{2}\left(\alpha + \frac{\lambda_{1,2}}{3}\right)\right) \tag{25}$$

where $\alpha = (82+63\cos(\mathrm{p})-18\cos(2\mathrm{p})+\cos(3\mathrm{p}))/128$ in which $p = m \cdot \Delta x$ ($0 \le p \le \pi$) is a dimensionless wave number, and

$$\lambda_{1,2} = \frac{1}{8}\mathrm{i}\delta d + \frac{1}{6}\mathrm{Df}\gamma \pm \frac{1}{24}\sqrt{-9\delta^2 a^2 + 16\mathrm{Df}^2\gamma^2}$$

where $\delta = \sin(2\mathrm{p}) - 10\sin(\mathrm{p})$, $d = a \cdot \mathrm{Fr}$ in which $a = \mathrm{Cr}/(\mathrm{Fr} \pm 1)$ and $\mathrm{Cr} = (U \pm c)\Delta t/\Delta x$ is the Courant number, and $\mathrm{Fr} = U/c$ is the Froude number, $\mathrm{Df} = r \cdot \Delta t$ is the dimensionless friction parameter, and $\gamma = \cos(\mathrm{p}) + 2$.

From the complex values $g_{n_{1,2}}$ (Eq. (25)), the modulus $|g_{n_{1,2}}|$ and the corresponding phase angles $\phi_{n_{1,2}} = -\arg(g_{n_{1,2}})$ are obtained. For the stability, according to von Neumann's condition, the requirement is $|g_{n_{1,2}}| \le 1$ for all p. For the accuracy, the convergence ratio $R_d = |g_n|/|g_a|$ and $R_c = \phi_n/\phi_a$, which measures dissipation and dispersion, respectively, for the principal progressive waves, for variations of Cr, Fr and Df, are evaluated. In Fig. 1, in polar coordinates, for Fr = 0.5, Df = 0, and Cr = 0.5, 1, and 1.5, R_d and R_c are plotted, respectively. In Fig. 2, the same numerical properties are presented for Cr = 0.5, Fr = 0.5, and Df = 0.001, 0.01, and 0.05. From Fig. 1(b) we can see that by increasing the Courant's number, there is an increase of the phase errors, while as it can be seen in Fig. 2(a) an antidissipative and unstable behaviour of the scheme is noticed by increasing the frictional parameter. It can be said that the dispersive effects are made less evident by the diffusion introduced by the ϑ_j limiter,

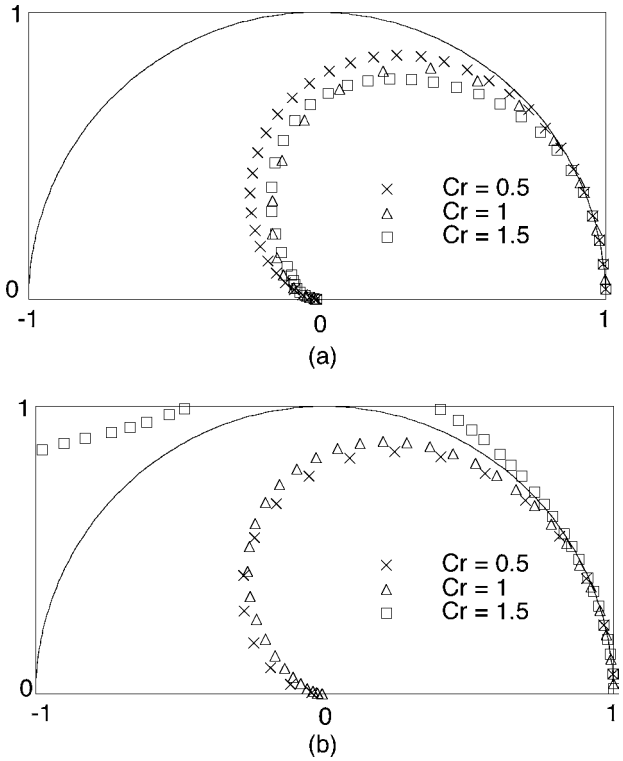

Figure 1 Amplitude ratio R_d (a), and celerity ratio R_c (b) for progressive waves with Fr = 0.5, Df = 0, and Cr = 0.5, 1, and 1.5.

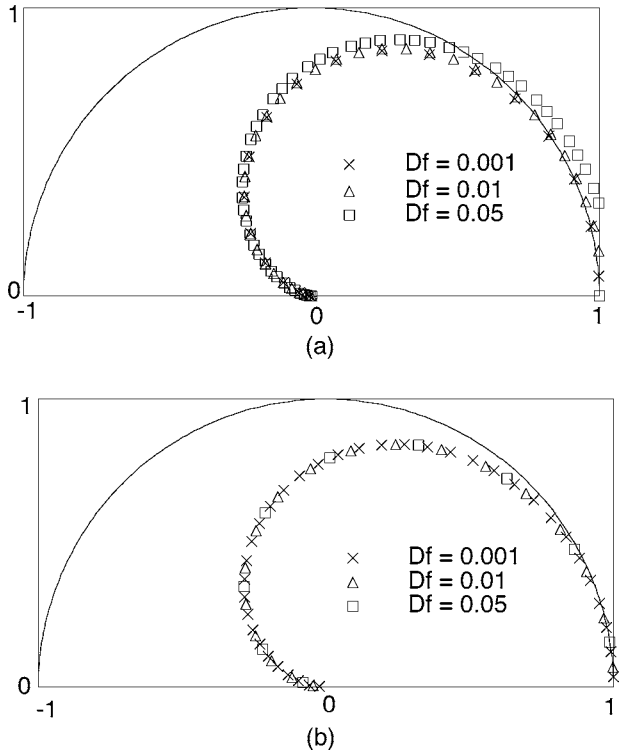

Figure 2 Amplitude ratio R_d (a), and celerity ratio R_c (b) for progressive waves with Cr = 0.5, Fr = 0.5, and Df = 0.001, 0.01, and 0.05.

specifically designed in order to prevent oscillations (Bianco *et al.*, 1999; Kurganov and Petrova, 2001). Finally, the variations of the Froude's number are resulted uninfluential.

4 Numerical applications

The third-order model proposed, indicated by T3_3 in the numerical tests, is applied for the representation of the shock phenomenon in open channels. In particular, the dam-break phenomenon in a rectangular, horizontal, and frictionless channel and the hydraulic jump in the channels with variable bed slope are simulated. The same tests cases are also carried out with first- and second-order models, indicated by T3_1 and T3_2, respectively. The numerical results are compared with the corresponding analytical solutions. In each test the L_2–relative error is evaluated in the form

$$\delta_h = \left[\frac{\sum_{j=1,N}(h^n - h^{ex})^2}{\sum_{j=1,N}(h^{ex})^2}\right]^{1/2} \times 100 \tag{26}$$

where, h^n and h^{ex} are the simulated and the exact depth, respectively, and N is the grid-point. The same evaluation is carried out for the velocity with the determination of the parameter δ_U. Moreover, a hydraulic jump problem compared with laboratory experiments is presented.

4.1 Idealized dam-break problem

A rectangular, horizontal, and frictionless channel, having a length of $L = 400$ m is considered. At the middle length of

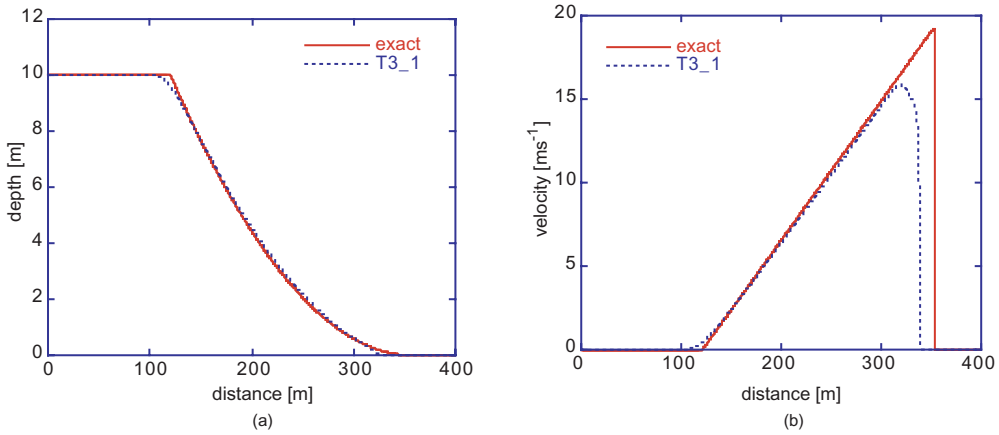

Figure 3 Water profile (a), and velocity (b), for T3_1 scheme, at $t = 8$ s, and for $N = 800$.

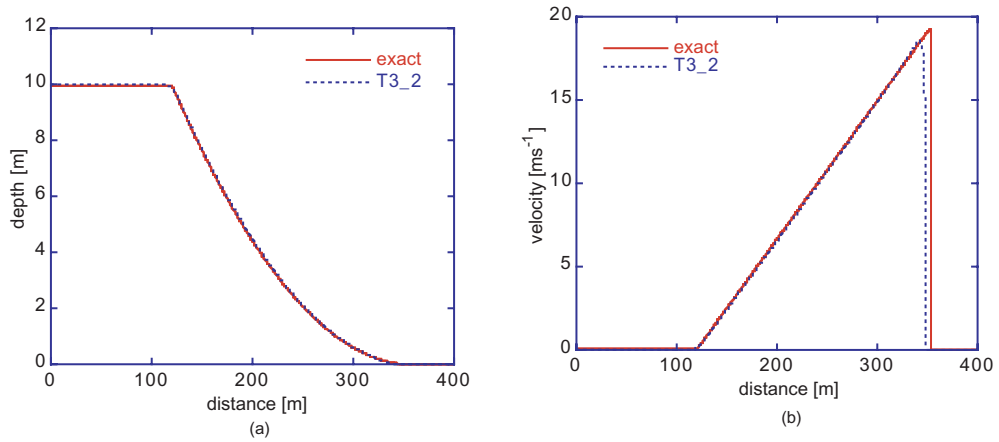

Figure 4 Water profile (a), and velocity (b), for T3_2 scheme, at $t = 8$ s, and for $N = 800$.

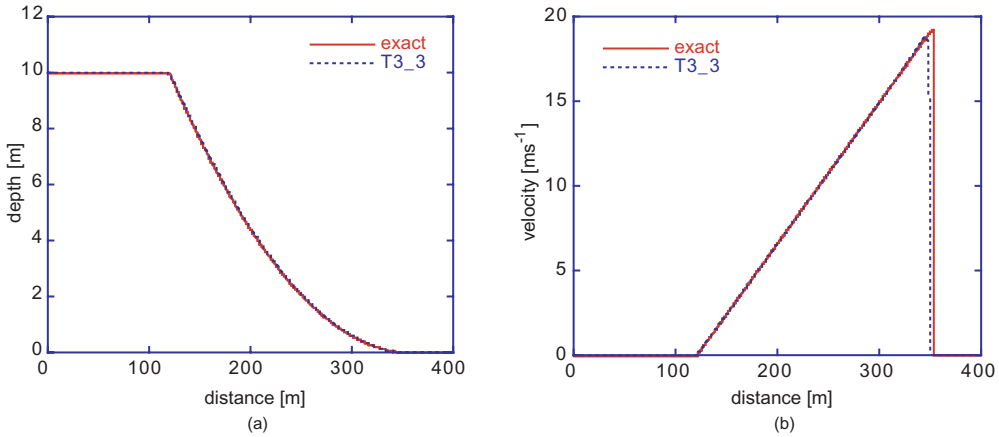

Figure 5 Water profile (a), and velocity (b), for T3_3 scheme, at $t = 8$ s, and for $N = 800$.

the channel is initially located a dam. Upstream the dam, the water depth is $h_0(x) = 10$ m and downstream is $h_0(x) = 0$. The boundary conditions, are set equal to the initial depth. At instant $t = 0$, the dam is removed instantaneously and the water depth and the velocity profiles obtained, at $t = 8$ s and for $N = 800$, with the schemes T3_1, T3_2, and T3_3, respectively, are compared with the analytical solution (Stoker, 1957) in Figs 3–5. In the simulations, a Courant number Cr $= 0.9$, is used. In Tables 1 and 2, we list the errors in function of the grid points N, δ_h, and δ_U, at $t = 8$ s, respectively.

Table 1 Errors δ_h, at $t = 8$ s, for the various scheme

N	T3_1	T3_2	T3_3
100	4.868370	2.147092	1.909964
200	3.256245	1.130954	9.8283E-1
400	2.130403	5.9839E-1	5.0599E-1
800	1.360632	3.1673E-1	2.5387E-1
1600	8.4726E-1	1.6323E-1	1.3108E-1
3200	5.1269E-1	8.2759E-2	6.7162E-2
6400	3.0988E-1	4.2139E-2	3.4519E-2

Table 2 Errors δ_U, at $t = 8$ s, for the various scheme

N	T3_1	T3_2	T3_3
100	40.393074	18.596095	13.397068
200	41.755968	22.832215	25.113128
400	44.057745	29.199830	25.029628
800	43.772737	26.903339	21.393447
1600	41.124108	22.528086	17.632018
3200	37.739001	17.725224	12.217187
6400	33.968592	13.038395	8.084848

4.2 *Super-sub-supercritical flow in rectangular channel*

In a rectangular channel, with a width $b = 10$ m and a length $L = 100$ m, the constant discharge is $Q = 20\,\mathrm{m^3/s}$ and the Manning's roughness coefficient is $n_m = 0.03\,\mathrm{m^{-1/3}\,s}$. The initial depth is $h_0(x) = 0.70658$ m, and the boundary conditions are $Q(0,t) = 20\,\mathrm{m^3/s}$ and $h(L,t) = 0.61803$ m. The analytical solution (MacDonald, 1994), which results to be supercritical at inflow and outflow and subcritical in $33.30 \le x \le 55.90$ m, is presented in Fig. 6.

In Fig. 7, at $t = 150$ s, and for $N = 400$, the water surface profile, for the schemes T3_1 (a), T3_2 (b), and T3_3 (c) are presented. Cr $= 0.6$ has been taken, so the friction parameter results Df $= 0.0087$ for $N = 50$, and diminuishes linearly with

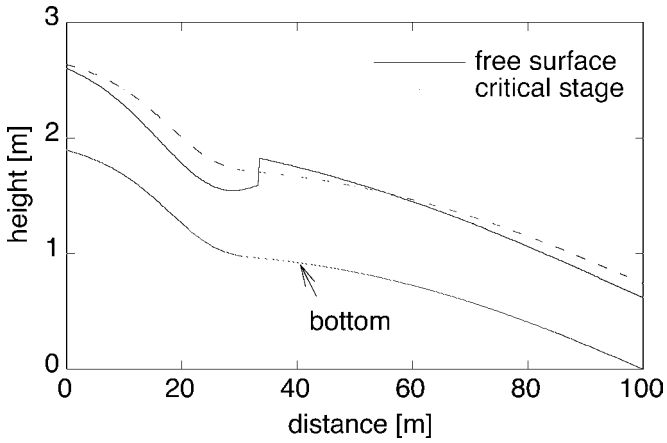

Figure 6 Exact solution.

Δx. In Table 3, at $t = 150$ s, the errors δ_h obtained for the three schemes are reported.

4.3 *Super-subcritical flow in non-uniform rectangular channel*

For this test problem, with $L = 1000$ m and $n_m = 0.02\,\mathrm{m^{-1/3}\,s}$, the channel is non-uniform rectangular with a variable width represented in Fig. 8, and given by

$$b(x) = 10 - 64\left[\left(\frac{x}{1000}\right)^2 - 2\left(\frac{x}{1000}\right)^3 + \left(\frac{x}{1000}\right)^4\right] \quad (27)$$

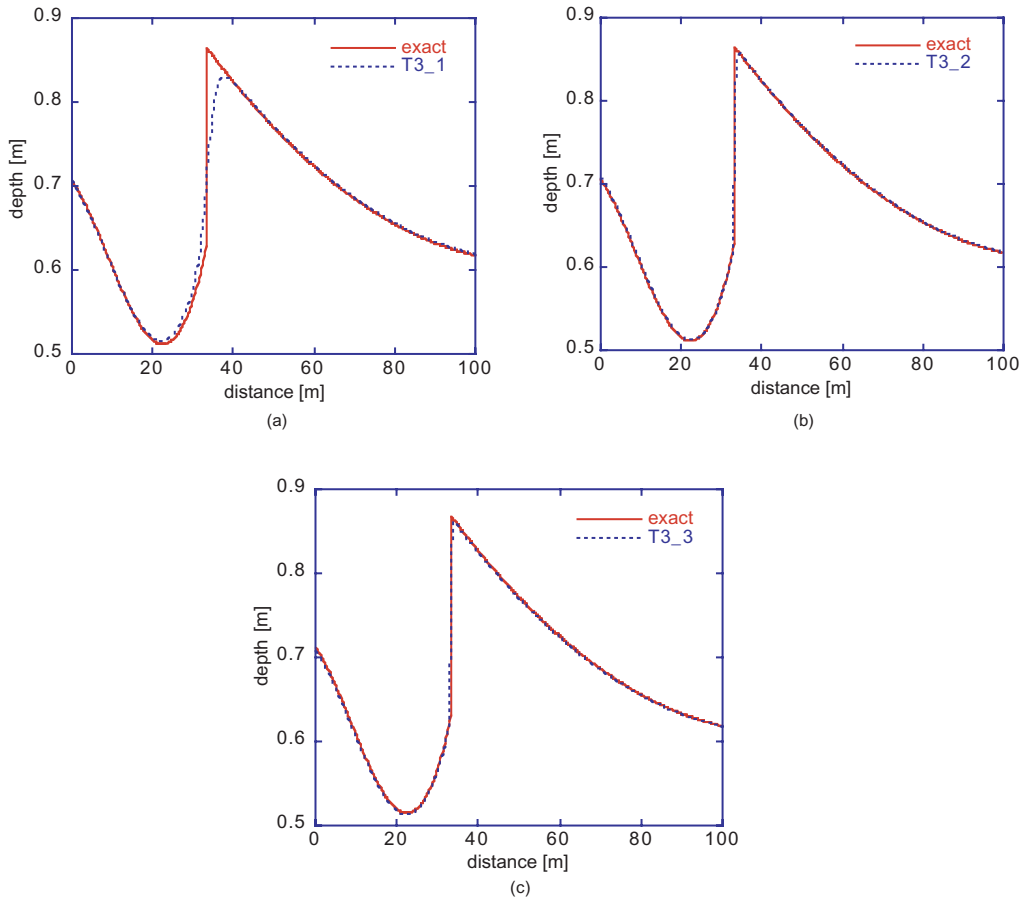

Figure 7 Water profile, at $t = 150$ s, and for $N = 400$, for T3_1 (a), T3_2 (b), and T3_3 (c) scheme.

Table 3 Errors δ_h, at $t = 150$ s, for the various scheme

N	T3_1	T3_2	T3_3
50	6.056640	2.836925	2.719853
100	4.470934	1.782015	1.551233
200	3.477099	1.290539	1.261008
400	2.505920	8.8593E-1	7.9954E-1
800	1.878940	6.6515E-1	6.4382E-1
1600	1.316577	4.4425E-1	4.0329E-1
3200	9.6602E-1	3.3669E-1	3.2274E-1

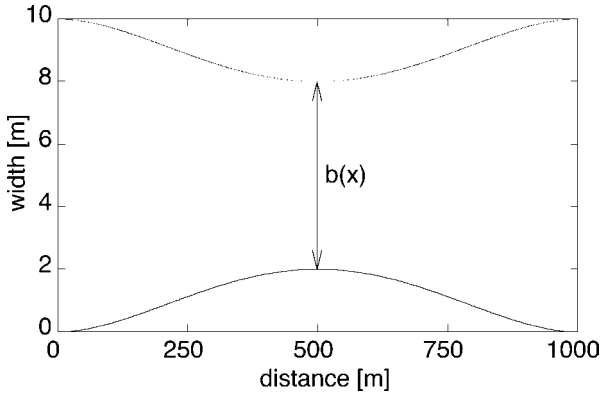

Figure 8 Channel with variable width.

A constant discharge $Q = 20\,\mathrm{m}^3/\mathrm{s}$ and an initial depth $h_0(x) = 0.64167$ m are assumed for the tests. The boundary conditions are $h(0,t) = 0.64167$ m and $h(L,t) = 1.125$ m. The analytical solution (MacDonald *et al.*, 1995) is supercritical at inflow and changes, via hydraulic jump at $x = 500$ m, to subcritical (Fig. 9).

In Fig. 10, at $t = 1000$ s and for $N = 1000$, for $470 \le x \le 530$ m, the water surface profile for the schemes T3_1, and T3_3 are presented. Taken Cr $= 0.6$, with $b(x)$ given by Eq. (27), it results $0.0095 \le$ Df ≤ 0.011 for $N = 250$. In Table 4, at $t = 1000$ s, the values δ_h for the three schemes are reported.

4.4 Hydraulic jump problem with measured data

For this test, a rectangular horizontal channel, with $L = 14$ m and $b = 0.46$ m, used for the experiments by Gharangik and Chaudhry (1991) is assumed. In the first simulations, with a Froude number Fr $= 4.23$, the initial conditions are $h_0(x) = 0.043$ m and $U_0(x) = 2.737$ m/s. The boundary conditions are $h(0,t) = 0.043$ m, $U(0,t) = 2.737$ m/s and $h(L,t) = 0.222$ m. Manning's roughness coefficient has been taken $n_m = 0.0075\,\mathrm{m}^{-1/3}$s, the space interval $\Delta x = 0.1$ m, and the Courant number Cr $= 0.6$, so Df $= 0.00178$ results. In Fig. 11, the steady-state profiles, computed at $t = 150$ s, with T3_1 and T3_3 schemes are presented in the shock region, with measured data.

Later, with Fr $= 6.65$, the initial and boundary conditions are $h_0(x) = 0.024$ m, $U_0(x) = 3.255$ m/s, $h(0,t) = 0.024$ m, $U(0,t) = 3.255$ m/s, and $h(L,t) = 0.195$ m. Taken $n_m = 0.0070\,\mathrm{m}^{-1/3}$ s, $\Delta x = 0.1$ m, Cr $= 0.6$, Df $= 0.00362$ results. The steady-state profiles, at $t = 150$ s, for these simulations are shown in Fig. 12.

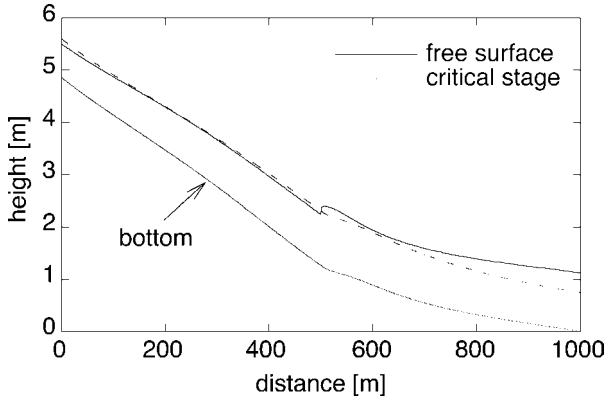

Figure 9 Exact solution.

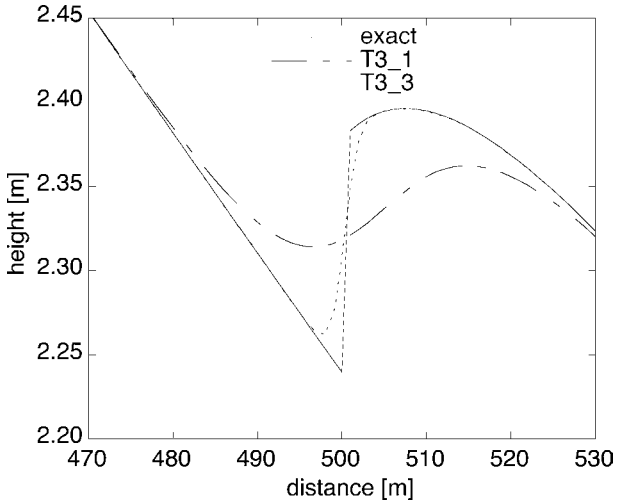

Figure 10 Water profile, at $t = 1000$ s, and for $N = 1000$, at $470 \le x \le 530$ m, for T3_1, and T3_3 schemes.

Table 4 Errors δ_h, at $t = 1000$ s, for the various scheme

N	T3_1	T3_2	T3_3
250	1.576129	6.3492E-1	5.9061E-1
500	1.146651	4.1781E-1	3.8890E-1
1000	8.1590E-1	2.8871E-1	2.6699E-1
2000	5.7832E-1	2.0407E-1	1.8666E-1
4000	4.1161E-1	1.4465E-1	1.3119E-1
8000	2.9373E-1	1.0397E-1	9.4615E-2

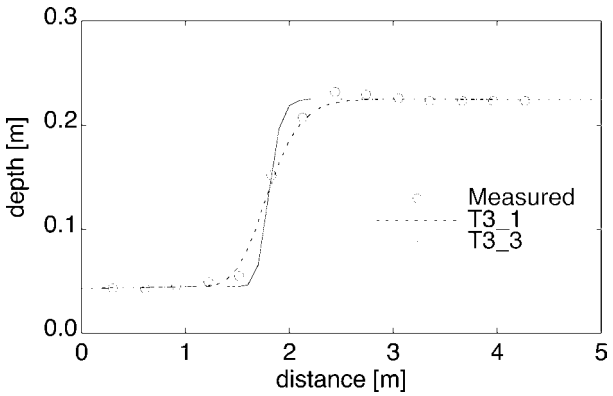

Figure 11 Hydraulic jump profiles for Fr $= 4.23$.

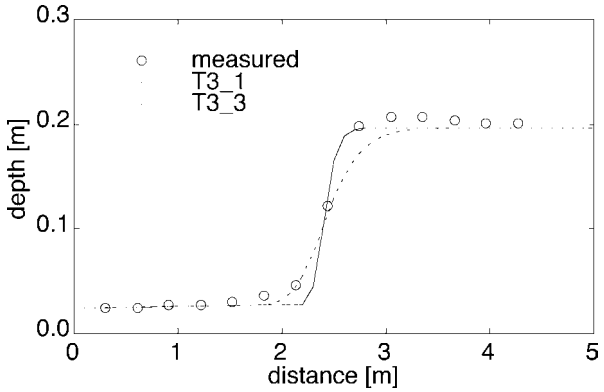

Figure 12 Hydraulic jump profiles for Fr = 6.65.

5 Conclusions

A third-order numerical model for the solution of non-homogeneous system of Saint-Venant equations, governing open-channel flow, has been proposed. The time explicit discretization has been obtained by Taylor series expansion in a factorized form. The space integration, following Godunov-type central scheme approach, has been carried out by using piecewise-quadratic polynomial. The stability analysis and the numerical properties have been studied. In particular, dispersion errors, by increasing the Courant number and instability, which is consequent to the antidissipation by increasing the friction parameter have been detected. However, in the model, this effects are limited from the flux limiter introduced. The numerical simulations, carried out in extreme conditions deal with dam-break, in a horizontal and frictionless channel, hydraulic jump phenomenon in prismatic and non-prismatic channels with bed topography, and in laboratory channels, shows the high-resolution representations obtained by the third-order scheme here proposed.

Notation

A = Cross-sectional area
b = Free-surface width
c = Celerity
Cr = Courant number
Df = Dimensionless friction parameter
f = Flux vector
Fr = Froude number
g = Gravitational acceleration
g_a, g_n = Analytical and numerical amplification factor
h = Water depth
i = Imaginary unit
I_1, I_2 = Pressure force integrals
J = Jacobian matrix of the flux vector
K = Matrix of the source terms
L = Length of simulation domain
n_m = Roughness coefficient of Manning's formula
m = Dimensional wave number
P = Wetted-perimeter
p = Dimensionless wave number
Q = Discharge
R = Hydraulic radius
r = Dimensional friction parameter
R_c, R_d = Celerity and amplitude ratio
S_0, S_f = Bottom and friction slope
t, x = Time and space
U = Mean velocity
u = Flow variables vector
z = Source terms vector
β = Temporal frequency
δ = Relative L_2-error defined by Eq. (26)
Δt, Δx = Time and space interval
η = Height above the bed channel
ϑ = Non-linear limiter defined by Eq. (13)
λ = Mesh ratio
σ = Channel width at distance η from bed
ϕ_a, ϕ_n = Analytical and numerical phase angle
Ω = Spatial domain.

References

1. BIANCO, F., PUPPO, G. and RUSSO, G. (1999). "High-order Central Schemes for Hyperbolic Systems of Conservation Laws". *SIAM J. Sci. Comput*. 21(1), 294–322.
2. BUTCHER, J.C. (1987). *The Numerical Analysis of Ordinary Differential Equations*. Wiley, New York.
3. CUNGE, J.A., HOLLY, Jr F.M. and VERWEY, A. (1980). *Practical Aspects of Computational River Hydraulics*. Pitman, London.
4. DELIS, A.I. and SKEELS, C.P. (1998). "TVD Schemes for Open Channel Flow". *Int. J. Numer. Methods Fluids* 26, 791–809.
5. DELIS, A.I., SKEELS, C.P. and RYRIE, S.C. (2000a). "Evaluation of Some Approximate Riemann Solvers for Transient Open Channel Flows". *J. Hydraul. Res*. 38(3), 217–231.
6. DELIS, A.I., SKEELS, C.P. and RYRIE, S.C. (2000b). "Implicit High-resolution Methods for Modeling One-dimensional Open Channel Flow". *J. Hydraul. Res.* 38(5), 369–382.
7. DONEA, J., ROIG, B. and HUERTA, A. (2000). "High-order Accurate Time-stepping Schemes for Convection-diffusion Problems". *Comput. Methods Appl. Mech. Eng.* 182, 249–275.
8. FRIEDRICHS, K.O. (1954). "Symmetric Hyperbolic Linear Differential Equations". *Comm. Pure Appl. Math.* VII, 345–392.
9. GHARANGIK, A.M. and CHAUDHRY, M.H. (1991). "Numerical Simulation of Hydraulic Jump". *J. Hydraul. Eng.* ASCE 117(9), 1195–1211.
10. HARTEN, A. (1983). "High Resolution Schemes for Hyperbolic Conservation Laws". *J. Comput. Phys.* 49, 357–393.
11. HIRSCH, C. (1995). *Numerical Computation of Internal and External Flows*, vol. 2. John Wiley & Sons, Chichester.
12. JHA, A.K., AKIYAMA, J. and URA, M. (1995). "First- and Second-order Flux Difference Splitting Schemes for Dam-break Problem". *J. Hydraul. Eng.* ASCE 121(12), 877–884.

13. KURGANOV, A. and PETROVA, G. (2001). "A Third-order Semi-discrete Genuinely Multidimensional Central Scheme for Hyperbolic Conservation Laws and Related Problems". *Numer. Math*. 88, 683–729.
14. KURGANOV, A. and TADMOR, E. (2000). "New High-Resolution Central Schemes for Nonlinear Conservation Laws and Convection–Diffusion Equations". *J. Comput. Phys.* 160, 241–282.
15. LAX, P.D. (1954). "Weak Solutions of Nonlinear Hyperbolic Equations and Their Numerical Computation". *Comm. Pure Appl. Math*. VII, 159–193.
16. van LEER, B. (1979). "Towards the Ultimate Conservative Difference Scheme. V. A Second-Order Sequel to Godunov's Methods". *J. Comput. Phys*. 32, 101–136.
17. LIU, X.-D. and OSHER, S. (1996). "Nonoscillatory High Order Accurate Self-similar Maximum Principle Satisfying Shock Capturing Schemes I". *SIAM J. Numer. Anal*. 33(2), 760–779.
18. LIU, X.D. and TADMOR, E. (1998). "Third Order Nonoscillatory Central Scheme for Hyperbolic Conservation Laws". *Numer. Math*. 79, 397–425.
19. MACDONALD, I. (1994). "Test Problems with Analytic Solutions for Steady Open Channel Flow". Numerical Analysis Report 6/94, Department of Mathematics, University of Reading.
20. MACDONALD, I., BAINES, M.J., NICHOLS, N.K. and SAMUELS, P.G. (1995). "Comparison of Some Steady State Saint-Venant Solvers for Some Test Problems with Analytic Solutions". Numerical Analysis Report 2/95, Department of Mathematics, University of Reading.
21. NESSYAHU, H. and TADMOR, E. (1990). "Non-oscillatory Central Differencing for Hyperbolic Conservation Laws". *J. Comput. Phys.* 87, 408–463.
22. SANDERS, B.F. (2001). "High-resolution and Non-oscillatory Solution of the St. Venant Equations in Non-rectangular and Non-prismatic Channels". *J. Hydraul. Res.* 39(3), 321–330.
23. STOKER, J.J. (1957). *Water Waves*. Interscience Publishers, New York.
24. TSENG, M.H., HSU, C.A. and CHU, C.R. (2001). "Channel Routing in Open-channel Flows with Surges". *J. Hydraul. Eng.* ASCE 127(2), 115–122.
25. WESSELING, P. (2001). *Principles of Computational Fluid Dynamics*. Springer, Berlin.